Mismatched Complementary-on-Receive Filtering of Diverse FM Waveform Subsets

Christian C. Jones and Shannon D. Blunt
Radar Systems Lab (RSL), University of Kansas, Lawrence, KS, USA

***Abstract*—The notion of complementary coding is generally thought to be a waveform design problem. In contrast, here we show that, for arbitrary diverse FM waveforms over the coherent processing interval (CPI), least-squares mismatched filters can be jointly computed to provide complementary sidelobe cancellation on receive when pre-summing of unique waveform subsets is performed after pulse compression (before Doppler processing). The efficacy of this scheme is demonstrated in simulation and with experimental free-space measurements.**

***Keywords*—complementary coding, mismatched filtering, waveform diversity, FM noise waveforms**

I. Introduction

Complementary codes were originally proposed by Golay [1] and have since been explored extensively (e.g. [2-5]) as a means to (theoretically) achieve complete sidelobe removal. Of course, it is well known that such codes are rather sensitive to Doppler effects, which is further exacerbated by the distortion that codes encounter when generated by a real transmitter [6, 7].

It was recently experimentally demonstrated in [8] that subsets of complementary FM waveforms combined via pre-summing on receive are more robust to Doppler and transmitter distortion effects than their code counterparts. Further, when the subsets themselves are unique across the CPI this complementary form of the broader category of FM noise waveforms [9-14] can achieve significant practical sidelobe suppression as well as inherently address the issue of range sidelobe modulation (RSM) of clutter that arises for agile waveforms [15-17].

Here instead of designing the waveforms to possess a complementary property we rely on the degrees of freedom provided by an arbitrary diverse set of nonrepeating FM waveforms to formulate collections of jointly designed mismatched filters (MMFs) so that the complementary property is still achieved. Generalizing the FM form of the Least Squares (LS) MMF developed in [6, 18] to the pre-summed result of Q pulse compression responses of distinct waveforms realizes a set of mismatched complementary-on-receive filters (MiCRFt) − pronounced the same as the elder brother of Sherlock Holmes − that facilitate this sidelobe suppression capability. It is further shown that a straightforward extension of this formulation provides a way in which to compensate for range straddling effects [19].

II. LS MMF for FM Waveforms

The LS MMF was originally developed for phase codes [20], though codes have practical limitations with regard to implementation on real radar systems due to an extended "spectral skirt" [21] that may easily exceed the passband of the transmitter. In contrast, FM waveforms can possess much better spectral containment because their continuous nature avoids the abrupt changes evidenced by phase codes (along with the recurring amplitude nulls that occur in the pulse envelope when physically implementing a phase code) [7]. Consequently, FM waveforms are far more suitable to generation at high power since they are more amenable to the rigors of a high power amplifier (HPA).

To attain the same sidelobe suppression benefit that the original LS MMF achieved for phase codes, in [6, 18] this optimal MMF formulation was modified for use with FM waveforms. The key distinction is that, while the phase-code MMF only relied on use of the discrete phase sequence, the FM form requires a sufficiently high-fidelity discretization of the continuous FM waveform that is achieved via "over-sampling" relative to the passband (since not bandlimited). However, this high-fidelity representation has the undesired outcome of a super-resolution condition that incurs severe mismatch loss (20 dB has been observed). To compensate, the LS MMF for FM waveforms is modified [6, 18] to produce a "beam-spoiling" effect that realizes roughly the nominal matched filter resolution, while still benefiting from substantially lower range sidelobes and low mismatch loss.

Let $s(t)$ denote an arbitrary FM waveform that has pulsewidth T and 3-dB bandwidth B, so BT is the waveform time-bandwidth product (defined relative to the passband bandwidth). To achieve the required fidelity this waveform is discretized with sampling period

$$T_{\mathrm{S}} = \frac{T}{K(BT)} = \frac{T}{N}\,, \tag{1}$$

where K is the over-sampling factor and N is the length of the resulting vector $\mathbf{s} = [s_1\ \ s_2\ \ \cdots\ \ s_N]^T$.

The original LS MMF formulation of [20] defines the $((M+1)N-1) \times MN$ convolution matrix

$$\mathbf{A} = \begin{bmatrix} s_1 & 0 & \cdots & 0 \\ \vdots & s_1 & & \vdots \\ s_N & \vdots & \ddots & 0 \\ 0 & s_N & & s_1 \\ \vdots & & \ddots & \vdots \\ 0 & \cdots & 0 & s_N \end{bmatrix}, \tag{2}$$

where MN is the length of the LS MMF (with M typically on the order of 2 to 4), to pose the desired relationship

$$\mathbf{A}\mathbf{h} = \mathbf{e}_m\,. \tag{3}$$

Here $\mathbf{e}_m$ is the length $(M+1)N-1$ elementary vector with a 1 in the mth element and zero elsewhere and $\mathbf{h}$ is the MMF. The well-known solution to (3) is [20]

$$\mathbf{h} = \left(\mathbf{A}^H \mathbf{A}\right)^{-1} \mathbf{A}^H \mathbf{e}_m \tag{4}$$

where $(\bullet)^H$ denotes the Hermitian operation.

To account for the over-sampling and associated beam-spoiled required for FM waveforms, [6, 18] modified the MMF in (4) as

$$\mathbf{h} = \left(\tilde{\mathbf{A}}^H \tilde{\mathbf{A}} + \delta \mathbf{I}\right)^{-1} \tilde{\mathbf{A}}^H \mathbf{e}_m\,, \tag{5}$$

where δ is a diagonal loading factor and $\mathbf{I}$ is a $MN \times MN$ identity matrix. Further, $\tilde{\mathbf{A}}$ is the same as the matrix $\mathbf{A}$ albeit

This work was supported by the Office of Naval Research under Contract #N00014-16-C-2029 and by a subcontract with Matrix Research, Inc. for the Air Force Research Laboratory under Prime Contract #FA8650-14-D-1722. DISTRIBUTION STATEMENT A. Approved for Public Release.

with some number of rows above and below the mth row replaced with zeros to provide the requisite beam-spoiling. The particular number of zeroed rows depends on the waveform, the value of K, and the acceptable degree of mismatch loss. It was shown in [9, 22] that beam-spoiling can alternatively be achieved by replacing the elementary vector in (4) with one containing only the mainlobe of the matched filter response (centered at the mth element) and zero elsewhere. Here we extend the FM-based LS MMF in (5) through a pre-summing receive arrangement to facilitate a set of MMFs that produce a complementary condition.

III. MiCRFt Formulation (Without Straddling)

The mismatched complementary-on-receive filtering (MiCRFt) approach given Q diverse FM waveforms (a contiguous subset within the CPI) is formulated by expanding the LS problem of (3) as

$$\sum_{q=1}^{Q} \tilde{\mathbf{A}}_q \mathbf{h}_q = Q\,\mathbf{e}_m\,, \tag{6}$$

where the scaling by Q accounts for coherent integration gain over the subset and the row-zeroed matrix $\tilde{\mathbf{A}}_q$ is used to address the FM waveform over-sampling for the qth discretized waveform $\mathbf{s}_q$. The form in (6) can then be rearranged as

$$\tilde{\mathbf{B}}\bar{\mathbf{h}} = Q\,\mathbf{e}_m \tag{7}$$

in which $\bar{\mathbf{h}} = [\mathbf{h}_1^T\ \mathbf{h}_2^T \cdots \mathbf{h}_Q^T]^T$ is an $MNQ \times 1$ composite of MMFs and the combined matrix $\tilde{\mathbf{B}} = [\tilde{\mathbf{A}}_1\ \tilde{\mathbf{A}}_2 \cdots \tilde{\mathbf{A}}_Q]$ has dimensionality $((M+1)N-1) \times MNQ$. Clearly (7) has the same general form as (3) and thus the collection of Q MiCRFt MMFs for this subset of FM waveforms can be obtained via the application of (5) as

$$\bar{\mathbf{h}} = Q\left(\tilde{\mathbf{B}}^H\tilde{\mathbf{B}} + \delta\bar{\mathbf{I}}\right)^{-1}\tilde{\mathbf{B}}^H\mathbf{e}_m\,, \tag{8}$$

where the matrix being inverted is $MNQ \times MNQ$, as is the expanded identity matrix $\bar{\mathbf{I}}$.

Note that the problem statement in (6) inherently relies on the use of Q diverse waveforms, such as the various forms of FM noise waveforms that have recently been demonstrated [9-14]. In the degenerate case in which all Q waveforms are identical, then (6) simplifies back to (3) and only a single MMF is realized. In other words, it is the additional degrees of freedom provided by this pulse agile form of waveform diversity that enables the complementary effect to be achieved. Further, one could expect possible degradation to occur due to ill-conditioning of (8) if the Q waveforms were too similar (e.g. small random perturbations of the same baseline waveform, such as could arise for [10] if the modulation index is low).

IV. Accounting for Range Straddling

Range straddling [19] (or range cusping [23]) is a well-known effect in which the discretized received response from a scatterer, after pulse compression, does not include the theoretical peak value of the mainlobe due to the continuum of possible delay shifts that could occur relative to the receive sampling process. For an optimized MMF, range straddling could significantly degrade sidelobe suppression capability if appropriate measures are not taken (i.e. waveforms with good spectral containment, sufficient "over-sampling" on receive, MMF diagonal loading and beamspoiling).

In [18] the version of LS MMF that had been proposed in [6] for FM waveforms was further modified to better account for range straddling effects through an arrangement that involved averaging of MMFs formed from different sampling offsets of the continuous waveform. Here we consider an alternative approach to facilitate incorporation into the MiCRFt formulation.

As in [18], segment the sampling period T_s from (1) into L equally-spaced delay offsets $\ell T_s/L$ for $\ell = 0, 1, \cdots, L-1$. Discretizing the continuous waveform $s(t)$ with the same sampling period T_s after introducing each of the relative delay offsets therefore produces the set of L length-N vectors $\mathbf{s}_{q,0}$, $\mathbf{s}_{q,1}$, …, $\mathbf{s}_{q,L-1}$ for the qth waveform.

For each of these sub-sample delay-offset versions of a given discretized waveform the MiCRFt LS problem in (6) can be written as

$$\sum_{q=1}^{Q} \tilde{\mathbf{A}}_{q,\ell}\,\mathbf{h}_q = Q\,\mathbf{e}_m\,, \tag{9}$$

where $\tilde{\mathbf{A}}_{q,\ell}$ is formed just like (2) with rows subsequently zeroed for the particular delay-offset vector $\mathbf{s}_{q,\ell}$. Note that the goal here is to realize a subset of MMFs $\mathbf{h}_q$ for $q = 1, 2, \cdots, Q$ that provide effectively the same response for a given scatterer regardless of sampling offset. Thus we can collect the L versions of (9) into a single representation akin to (7) via

$$\tilde{\mathbf{C}}\bar{\mathbf{h}} = Q\,\bar{\mathbf{e}}_m\,, \tag{10}$$

in which $\bar{\mathbf{e}}_m = [\mathbf{e}_m^T\ \mathbf{e}_m^T \cdots \mathbf{e}_m^T]^T$ is a length $((M+1)N-1)L$ vector that is a concatenation of L replicas of $\mathbf{e}_m$ and the matrix

$$\tilde{\mathbf{C}} = \begin{bmatrix} \tilde{\mathbf{A}}_{1,0} & \tilde{\mathbf{A}}_{2,0} & \cdots & \tilde{\mathbf{A}}_{Q,0} \\ \tilde{\mathbf{A}}_{1,1} & \tilde{\mathbf{A}}_{2,1} & \cdots & \tilde{\mathbf{A}}_{Q,1} \\ \vdots & \vdots & \ddots & \vdots \\ \tilde{\mathbf{A}}_{1,L-1} & \tilde{\mathbf{A}}_{2,L-1} & \cdots & \tilde{\mathbf{A}}_{Q,L-1} \end{bmatrix} \tag{11}$$

has dimensionality $((M+1)N-1)L \times MNQ$.

The solution to (10) follows directly from (8) as

$$\bar{\mathbf{h}} = Q\left(\tilde{\mathbf{C}}^H\tilde{\mathbf{C}} + \delta\bar{\mathbf{I}}\right)^{-1}\tilde{\mathbf{C}}^H\bar{\mathbf{e}}_m \tag{12}$$

for the identity matrix $\bar{\mathbf{I}}$ and corresponding matrix inverse having the same $MNQ \times MNQ$ dimensionality as (8). Thus the Q length-MN filters realized by (12) can be made robust to range straddling effects and also provide responses that realize complementary sidelobe cancellation when combined via pre-summing on receive.

Finally, it is clear that the $MNQ \times MNQ$ matrix inverse in (8) and (12) is daunting computationally even for modest time-bandwidth product waveforms. Our purpose here is to demonstrate what is possible and it remains to be seen whether this manner of receive processing can be made feasible in real-time (though processing capabilities do continue to grow at a rapid pace).

V. Mismatch Metric

As the name implies a mismatched filter (MMF) trades some of the SNR gain of the matched filter for lower range sidelobes. To assess the degree of mismatch loss (separate from straddling loss) we can first normalize each matched filter by $\mathbf{s}^H\mathbf{s}$, which for discretized FM waveforms of the same BT yields a constant value across all waveforms, so that the resulting noise gain is unity. Normalizing an MMF to likewise yield a unity noise gain can be accomplished via

$$\mathbf{h} = \frac{\mathbf{h}}{\sqrt{\left(\mathbf{h}^H\mathbf{h}\right)\left(\mathbf{s}^H\mathbf{s}\right)}}\,, \qquad (13)$$

with the mismatch loss the ratio of the MMF peak value to the MF peak value (which is also unity due to normalization). For agile waveforms this per-pulse mismatch loss is then simply averaged over the CPI.

For MiCRFt we wish to normalize the noise gain of the sum of the Q filter responses so that their relative scaling remains the same to preserve complementary sidelobe cancellation. Thus MiCRFt normalization is performed as

$$\bar{\mathbf{h}} = \frac{\bar{\mathbf{h}}}{\frac{1}{Q}\sqrt{\left(\sum_{q=1}^{Q}\mathbf{h}_q{}^H\mathbf{h}_q\right)\left(\sum_{q=1}^{Q}\mathbf{s}_q{}^H\mathbf{s}_q\right)}} = \frac{Q\,\bar{\mathbf{h}}}{\sqrt{\left(\bar{\mathbf{h}}^H\bar{\mathbf{h}}\right)\left(\bar{\mathbf{s}}^H\bar{\mathbf{s}}\right)}} \qquad (14)$$

where $\bar{\mathbf{s}} = [\mathbf{s}_1^T\ \mathbf{s}_2^T\ \cdots\ \mathbf{s}_Q^T]^T$. Hence the mismatch loss in this case involves the sum of the set of MiCRFt filter responses at the peak value divided by the sum of normalized MF peak responses over the same Q pulses. The latter value is Q for FM waveforms having the same BT. This ratio is then averaged over the pre-summed responses across the CPI.

VI. Simulation Analysis

To evaluate the efficacy of MiCRFt, random FM waveforms based on the frequency template error (FTE) approach [12] were generated to have a time-bandwidth product of $BT = 300$, with the discretized versions used for simulation assessment over-sampled by $K = 3$ (relative to 3-dB bandwidth B). We begin by assessing the sidelobe suppression achieved for a hypothetical noise-free point scatterer and the combination of $Q = 2$ responses via pre-summing. Here the MiCRFt formulation in (8) is used to form two filters using $M = 4$, $\delta = 1$, and zeroing $2K = 6$ rows above/below the mth row for beamspoiling. Standard matched filtering (MF) and the individual beamspoiled MMFs from (5) with the same parameters are also applied.

Figure 1 illustrates the significant sidelobe suppression benefit that MiCRFt provides relative to both the MFs and the individual FM-based LS MMFs from [6]. Of course, when worst-case range straddling occurs (Fig. 2) some degradation of the MiCRFt sidelobes arise, which can reasonably be expected since they were so low in Fig. 1. Moreover, Fig. 2 shows that for the straddling condition MiCRFt (using (8)) and the LS MMFs from [6] are negligibly different.

The form of MiCRFt in (12) that addresses range straddling was then applied using $L = 2$, such that a single delay offset version of each waveform at $0.5T_s$ was incorporated into the MMF design. Thus the point of maximum straddling now occurs at $0.25T_s$. Figure 3 shows this worst-case response using these compensated MMFs, where 7.4 dB in peak sidelobe suppression is regained.

Mismatch filtering and range straddling both produce some degree of mismatch loss. Table 1 compares the combined total mismatch loss for the different filtering schemes and straddling offset. While standard matched filtering experience no mismatch loss (by definition) in the absence of straddling, it does realize 0.8 dB at maximum straddling in this case. In fact, the version of MiCRFt from (12) using $L = 2$ actually exhibits the least worst-case straddling degradation among these filter pairs. It has also been observed that modest additional improvement in both sidelobe suppression and mismatch loss is obtained for MiCRFt as Q increases, though the same is not necessarily true for increasing L due to finite degrees-of-freedom.

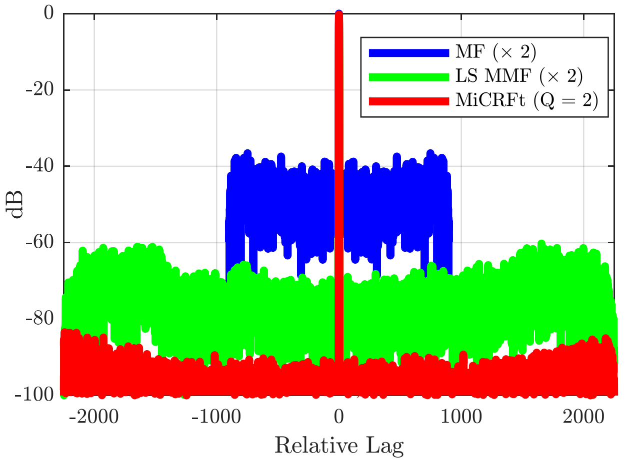

Fig. 1. Pulse compression responses after pre-summing of two random FM waveforms with no straddling (point scatterer without noise)

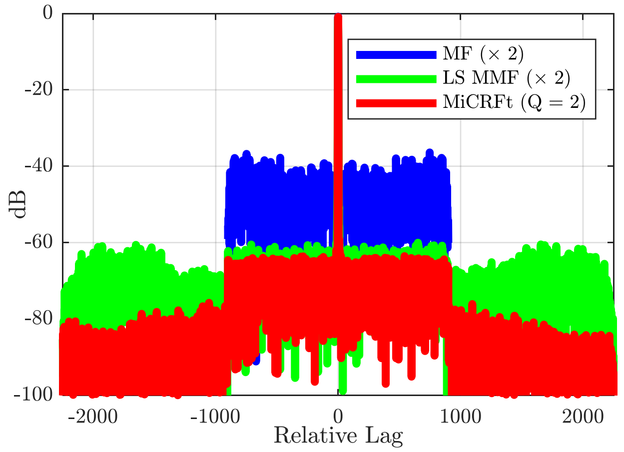

Fig. 2. Pulse compression responses after pre-summing of two random FM waveforms at maximum straddling of $0.5T_s$ (point scatterer without noise)

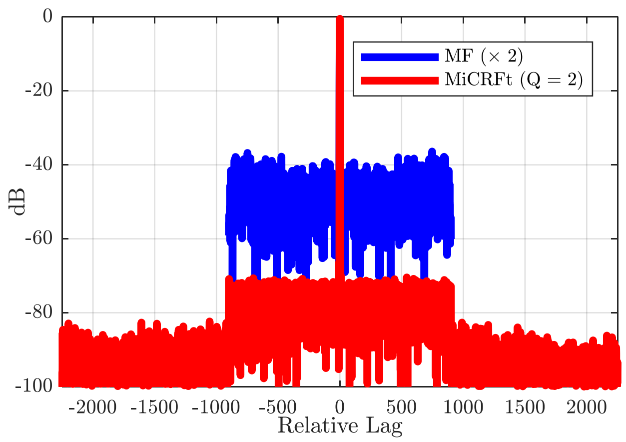

Fig. 3. Compensated MiCRFt from (12) for worst-case range straddling (point scatterer without noise)

TABLE I. TOTAL MISMATCH LOSS FOR TWO FTE [13] WAVEFORMS

Filter Type	Total Mismatch Loss		
	offset = 0T_s	**0.25T_s**	**0.5T_s**
MF	0 dB	0.2 dB	0.8 dB
LS MMF (5)	1.0 dB	1.1 dB	1.4 dB
MiCRFt (8)	0.2 dB	0.4 dB	0.9 dB
MiCRFt (12)	0.5 dB	0.3 dB	0.5 dB

To further study the trade-space of mismatch loss and sidelobe suppression, 3000 unique waveforms were created using a different random FM waveform design – temporal template error (TTE) [13] – to perform a Monte Carlo analysis of the average peak sidelobe level (PSL) and mismatch loss for different values of Q and L within the MiCRFt framework and different degrees of range straddling. Specifically, values of Q = 2 and 3 are considered, along with L = 1, 2, and 3. These different filter subsets were compared with standard MFs and the MMFs from (5) [6] at straddling offsets of 0.0T_s, 0.125T_s, 0.25T_s, 0.375T_s and 0.5T_s. All MMFs use the same diagonal loading, filter length, and beamspoiling as described above.

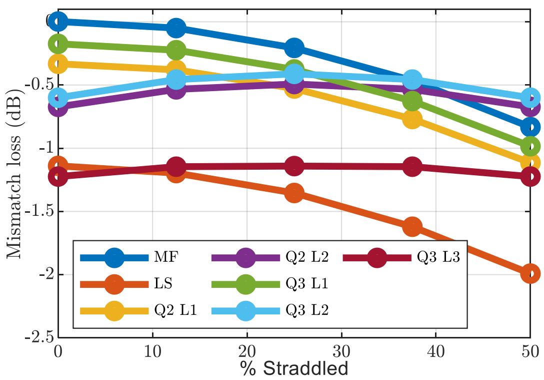

Fig. 4. Average mismatch loss vs percent straddled

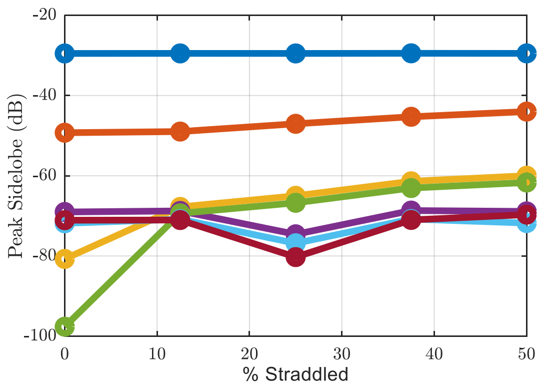

Fig. 5. Average PSL vs percent straddled

Figures 4 and 5 show the corresponding mismatch loss and PSL for each of these filter/straddling configurations (same color associations in each) where some interesting observations can be made. Relative to the degree of straddling offset, the L = 1 cases (yellow and green traces) follow the same mismatch loss trend in Fig. 4 as the MF (dark blue) and the individual LS MMFs (orange). Increasing the value of Q for the same L realizes a modest improvement in mismatch loss. However, increasing L produces a flattening across different offsets (as it was intended to do) that comes at the price of slightly greater mismatch loss when L exceeds 2 due to more design degrees of freedom being used to produce this flat response. That said, increasing both Q and L provide better PSL (Fig. 5), albeit with clearly diminishing improvements.

VII. EXPERIMENTAL RESULTS

Finally, the MiCRFt formulation was applied to free-space measurements to assess whether the performance obtained in simulation can be realized in real data. Here another set of TTE waveforms [13] were transmitted from the roof of Nichols Hall on the University of Kansas campus. In this case 1000 unique TTE waveforms were generated with $BT = 150$ and $K = 3$. These waveforms were subsequently up-sampled and digitally up-converted to a center frequency of 3.55 MHz, loaded onto an arbitrary waveform generator (AWG), and used to illuminate the intersection of 23rd and Iowa Streets in Lawrence, KS where a fair amount of moving vehicles were present.

Again using Q = 2, L = 2, and M = 4, a single pair of MiCRFt filters was obtained via (12) for an arbitrary pair of the receive-captured responses (via a real-time spectrum analyzer). Figure 6 depicts the zero Doppler response for this filter pair along with the associated MFs and the individual MMFs from (5). The dominant response at a range of 0 m is the direct path that arises from using separate (yet collocated) transmit and receive antennas in a pseudo-monostatic configuration. Compared to the MFs (blue), the individual MMFs (green) provide greater visibility of the scatterers in the 300-600 m vicinity, though the extended MMF length also degrades visibility near the traffic intersection that resides at 1000-1200 m. In contrast, the greater sidelobe suppression of MiCRFt (red) provides enhanced visibility over the entirety of the range profile.

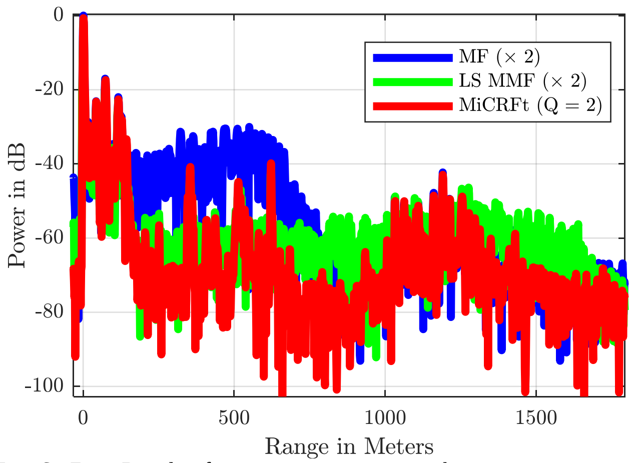

Fig. 6. Zero Doppler free-space measurement when pre-summing two arbitrary filtered responses

Forming the 1000 pulsed echoes into 500 pairs, the different filter responses can also be evaluated after Doppler processing. Here a Hamming window is applied to reduce Doppler sidelobes and a simple zero-Doppler projection form of clutter cancellation is used since the platform is stationary. The results are illustrated in Figs. 7-12, where Figs. 7-9 provide a close-up of the traffic in the intersection and Figs. 10-12 depict the entire range-Doppler scene.

Figures 7 and 10 serve as a performance baseline that shows the utility of random FM waveforms, albeit with the use of simple matched filtering. Consequently, despite the purpose of MMFs being the reduction of sidelobes, it is observed in Fig. 8 for the individually designed LS MMFs from (5) that the sidelobe level has actually increased relative to Fig. 7. The reason for this apparent degradation is that the factor of M = 4 length extension to the MMF (relative to the MF) is causing sidelobes from the large direct path to extend over a considerably greater distance. A comparison of the entire range-Doppler response in Figs. 10 and 11 for these same filter structures underscores this effect, where the LS MMFs have greatly reduced the direct path sidelobes, but at the expense of spreading them over a greater range interval.

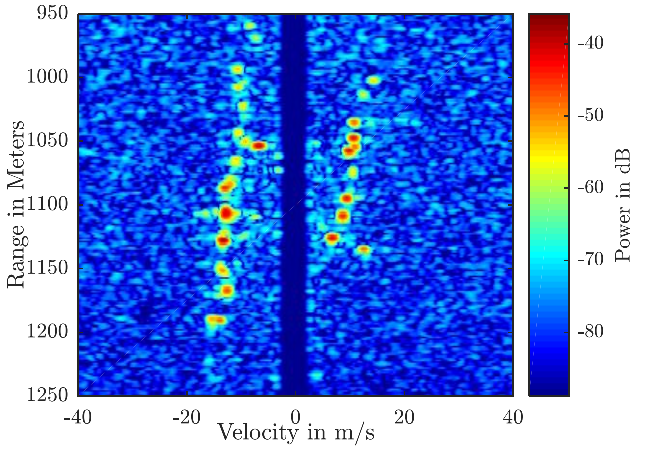

Fig. 7. Range-Doppler response of the intersection for 1000 TTE waveforms and MFs after pre-summing by 2

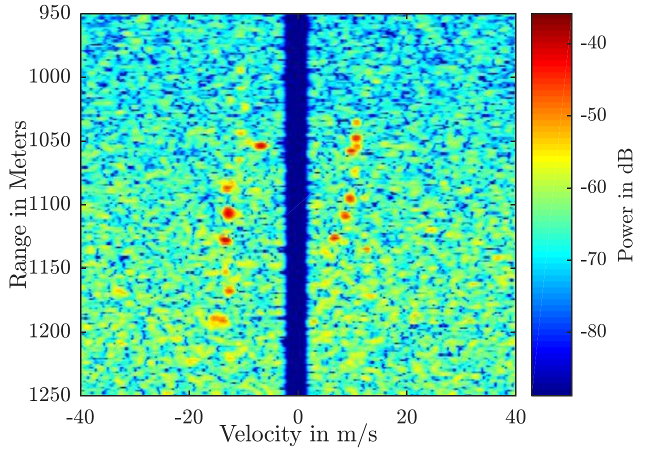

Fig. 8. Range-Doppler response of the intersection for 1000 TTE waveforms and LS MMFs from (5) after pre-summing by 2

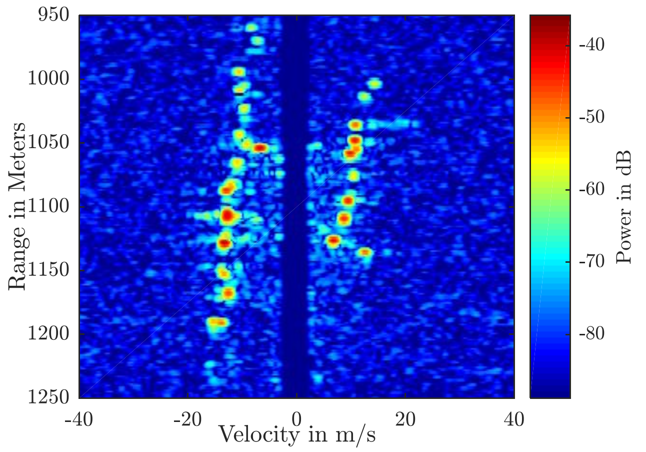

Fig. 9. Range-Doppler response of the intersection for 1000 TTE waveforms and MiCRFt from (12) with Q = 2 and L = 2

In contrast to these results, we see in Fig. 9 that MiCRFt has reduced the background sidelobes relative to the MFs. Moreover, it is observed in the associated Fig. 12 that the range-Doppler sidelobes have been nearly completely removed from the entire scene. Thus MiCRFt combined with diverse waveforms provides a rather effective means of suppressing sidelobes and, by extension, mitigating the effect of range sidelobe modulation (RSM) of clutter that smears across Doppler.

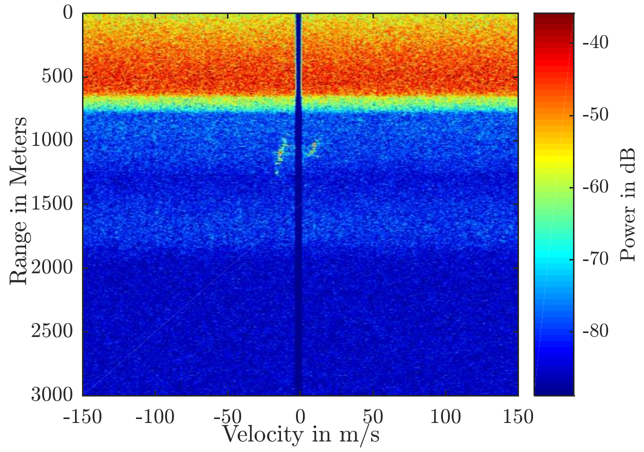

Fig. 10. Entire range-Doppler response for 1000 TTE waveforms and MFs after pre-summing by 2

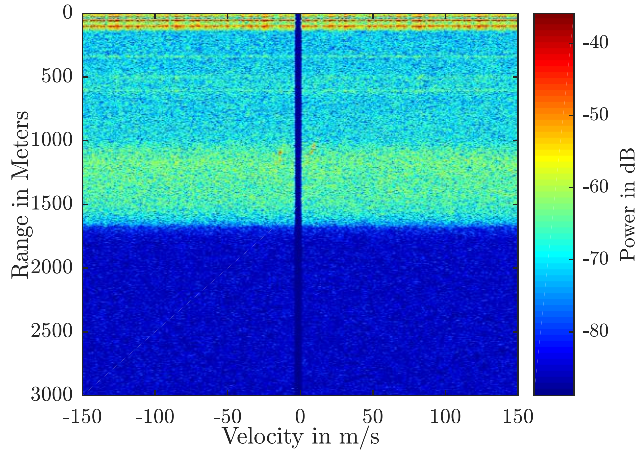

Fig. 11. Entire range-Doppler response for 1000 TTE waveforms and LS MMFs from (5) after pre-summing by 2

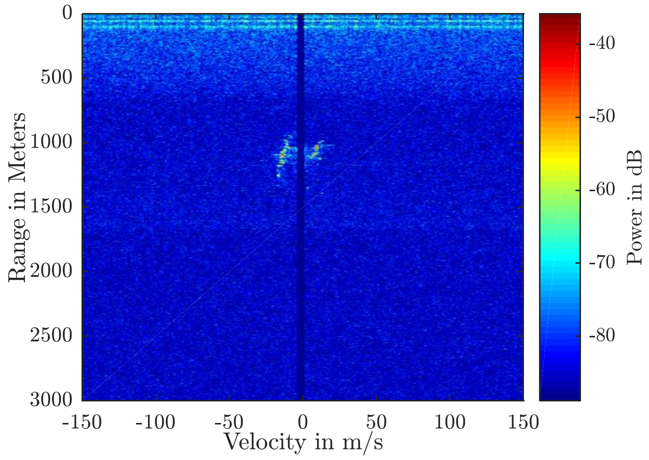

Fig. 12. Entire range-Doppler response for 1000 TTE waveforms and MiCRFt from (12) with Q = 2 and L = 2

VIII. Conclusions

It has been demonstrated via simulation and with experimental free-space measurements that a complementary form of mismatched filtering can be realized for arbitrary diverse FM waveforms. This new formulation has been compared to standard matched filtering and FM-based LS mismatch filtering (when computed individually), and has been shown to significantly outperform both. Of course, this enhanced performance comes at the cost of greater computational complexity and does require pre-summing on receive (with the associated Doppler space trade-off that is incurred). That said, the waveforms and corresponding filters could also be determined offline beforehand or in a parallel pipelined manner as needed if such resources exist.

References

[1] M.J.E. Golay, "Complementary series," *IRE Trans. Information Theory*, vol. IT-7, no. 2, pp. 82-87, Apr. 1961.

[2] R. Sivaswamy, "Multiphase complementary codes," *IEEE Trans. Information Theory*, vol. IT-24, no. 5, pp. 546-552, Sept. 1978.

[3] R.L. Frank, "Polyphase complementary codes," *IEEE Trans. Information Theory*, vol. IT-26, no. 6, pp. 641-647, Oct. 1980.

[4] A. Pezeshki, A.R. Calderbank, W. Moran, S.D. Howard, "Doppler resilient Golay complementary waveforms," *IEEE Trans. Information Theory*, vol. 54, no. 9, pp. 4254-4266, Sept. 2008.

[5] N. Levanon, I. Cohen, P. Itkin, "Complementary pair radar waveforms – evaluating and mitigating some drawbacks," *IEEE AESS Systems Magazine*, vol. 32, no. 3, pp. 40-50, Mar. 2017.

[6] S.D. Blunt, M. Cook, J. Jakabosky, J.D. Graaf, E. Perrins, "Polyphase-coded FM (PCFM) radar waveforms, part I: implementation," *IEEE Trans. Aerospace and Electronic Systems*, vol. 50, no. 3, pp. 2218-2229, July 2014.

[7] S.D. Blunt, E.L. Mokole, "An overview of radar waveform diversity," *IEEE AESS Systems Magazine*, vol. 31, no. 11, pp. 2-42, Nov. 2016.

[8] C.A. Mohr, P.M. McCormick, S.D. Blunt, "Optimized complementary waveform subsets within an FM noise radar CPI," *IEEE Radar Conf*., Oklahoma City, OK, USA, Apr. 2018.

[9] J. Jakabosky, S.D. Blunt, B. Himed, "Spectral-shape optimized FM noise radar for pulse agility," *IEEE Radar Conf.*, Philadelphia, PA, USA, May 2016.

[10] C. Sahin, J. Jakabosky, P. McCormick, J. Metcalf, S. Blunt, "A novel approach for embedding communication symbols into physical radar waveforms," *IEEE Radar Conf*., Seattle, WA, USA, May 2017.

[11] B. Ravenscroft, P.M. McCormick, S.D. Blunt, E. Perrins, J.G. Metcalf, "A power-efficient formulation of tandem-hopped radar & communications," *IEEE Radar Conf*., Oklahoma City, OK, USA, Apr. 2018.

[12] C.A. Mohr, P.M. McCormick, S.D. Blunt, C. Mott, "Spectrally-efficient FM noise radar waveforms optimized in the logarithmic domain," *IEEE Radar Conf*., Oklahoma City, OK, USA, Apr. 2018.

[13] C.A. Mohr, S.D. Blunt, "FM noise waveforms optimized according to a temporal template error (TTE) metric," *IEEE Radar Conf.*, Boston, MA, USA, Apr. 2019.

[14] C.A. Mohr, S.D. Blunt, "Design and generation of stochastically defined, pulsed FM noise waveforms," *Intl. Radar Conf.*, Toulon, France, Sept. 2019.

[15] S.D. Blunt, M.R. Cook, J. Stiles, "Embedding information into radar emissions via waveform implementation," *Intl. Waveform Diversity & Design Conf.*, Niagara Falls, Canada, Aug. 2010.

[16] C. Sahin, J. Metcalf, S. Blunt, "Characterization of range sidelobe modulation arising from radar-embedded communications," *IET Intl. Conf. Radar Systems*, Belfast, UK, Oct. 2017.

[17] A.C. O'Connor, J.M. Kantor, J. Jakabosky, "Filters that mitigate waveform modulation of radar clutter," *IET Radar, Sonar & Navigation*, vol. 11, no. 8, pp. 1188-1195, July 2017.

[18] D. Henke, P. McCormick, S.D. Blunt, T. Higgins, "Practical aspects of optimal mismatch filtering and adaptive pulse compression," *IEEE Intl. Radar Conf.*, Arlington, VA, USA, May 2015.

[19] M.A. Richards, J.A. Scheer, and W.A. Holm, *Principles of Modern Radar: Basic Principles*, SciTech Publishing, pp. 786-787, 2010.

[20] M.H. Ackroyd, F. Ghani, "Optimum mismatched filters for sidelobe suppression," *IEEE Trans. Aerospace and Electronic Systems*, vol. AES-9, no. 2, pp. 214-218, Mar. 1973.

[21] N. Levanon, E. Mozeson, *Radar Signals*, Wiley – IEEE Press, 2004.

[22] C. Sahin, J. Metcalf, S. Blunt, "Filter design to address range sidelobe modulation in transmit-encoded radar-embedded communications," *IEEE Radar Conf*., Seattle, WA, USA, May 2017.

[23] A.M. Klein, M.T. Fujita, "Detection performance of hard-limited phase-coded signals," *IEEE Trans. Aerospace & Electronic Systems*, vol. AES-15, no. 6, pp. 795-802, Nov. 1979.